Journal of Physics: Conference Series **1596** (2020) 012046 doi:10.1088/1742-6596/1596/1/012046

Diagnostics for Electron Pulse Trains at SwissFEL Obtained by Energy Modulation in a Laser-Driven Dielectric Structure

Benedikt Hermann[1,2,*], Simona Bettoni[1], Thilo Egenolf[3], Thomas Feurer[2], Franziska Frei[1], Uwe Niedermayer[3], Eduard Prat[1] and Rasmus Ischebeck[1]

[1] Paul Scherrer Institut, 5232 Villigen PSI, Switzerland
[2] Institute of Applied Physics, University of Bern, 3012 Bern, Switzerland
[3] Institute for Accelerator Science and Electromagnetic Fields (TEMF), TU Darmstadt, 64289 Darmstadt, Germany

E-mail: *benedikt.hermann@psi.ch

Abstract. Electron pulse trains with sub-femtosecond spike length offer novel possibilities to ultra-fast pump-probe experiments in free-electron lasers. The pulse train can be generated by an energy modulation which is converted to temporal bunching in a magnetic chicane. The source of the energy modulation is typically a resonant interaction with a co-propagating laser in a wiggler magnet. Alternatively, the modulation can be obtained by a dielectric laser accelerator (DLA). The implementation of the DLA modulation scheme at SwissFEL would be enabled by using the experimental chamber installed in the framework of the Accelerator-on-a-Chip International Program (ACHIP) and a magnetic chicane placed afterwards. In this contribution, we will focus on electron beam diagnostics for the DLA-modulated and compressed electron bunch train. Our simulation results predict that measuring the energy spread of the modulated beam and coherent diffraction radiation emitted from a foil with a hole provides a precise tool to characterize and optimize the laser-electron modulation. An absolute measurement of the longitudinal phase-space with a temporal rms-resolution of 350 as is possible with the planned X-band transverse deflecting cavity in Athos.

Introduction

Free-electron lasers (FELs) make use of a highly compressed relativistic electron beam to generate electromagnetic radiation in a magnetic undulator. They are the brightest sources of radiation from the VUV [1, 2] to the X-ray regime [3, 4, 5, 6, 7]. A technique proposed to generate an individual or a train of sub-femtosecond X-ray pulses with well-defined separation is the energy modulation of the electron bunch with a laser in the magnetic field of a resonant undulator (wiggler). The energy modulation is converted into a longitudinal density modulation with a magnetic chicane. This enhanced SASE (ESASE) method was proposed by Zholents [8], and has been implemented at LCLS and is planned at other facilities such as SwissFEL. As an alternative approach, we investigated and compared the modulation of the electron beam in a dielectric laser accelerator (DLA) to the conventional undulator modulation scheme. In a DLA, electrons interact with the near-field excited by an external laser in the vicinity of a dielectric micro-structure. The phase velocity of the evanescent wave depends on the periodicity

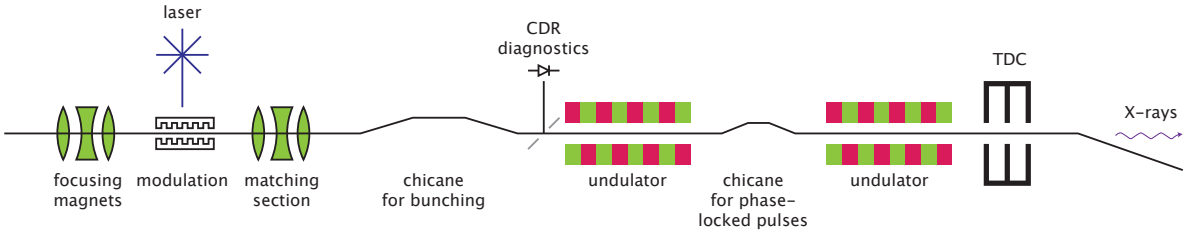

Figure 1. Sketch of the DLA modulation scheme. After modulation of the longitudinal phase-space, the ultra-relativistic electron beam is bunched in a magnetic chicane. The resulting pulse train creates uniformly spaced spikes of X-ray radiation in the undulator section. A coherent diffraction radiation (CDR) monitor after the bunching chicane can be used as a passive temporal diagnostic for the electron bunch. A direct measurement of the longitudinal phase-space is possible with a transverse deflecting cavity (TDC) at the end of the beamline. The illustration is adapted from [10].

of the structure and the wavelength of the laser. Resonant acceleration of electrons requires the phase velocity to match to the particles velocity (phase-synchronicity) [9]. Particles resonantly gain or lose energy depending on their phase. If the initial electron beam is longer than the wavelength of the driving laser, the longitudinal phase space will be modulated. In a beam dynamics simulation study, we estimate that a similar modulation strength can be achieved by around 10 times less laser power using the DLA scheme due to the reduced interaction volume. Further details on the DLA modulation concept for the generation of pulse trains in FELs can be found in [10]. The beamline required for the proposed scheme is sketched in Figure 1. The intrinsic synchronization of the FEL pulses to an external laser makes these schemes very suitable for ultra-fast pump-probe experiments. The CHIC scheme in the soft X-ray beamline in SwissFEL (Athos) makes use of magnetic chicanes between the undulator segments to delay the electron beam with respect to the X-rays [11]. This setup would allow the generation of a phase locked pulse train [12]. The vacuum chamber for the DLA interaction, which is equipped with a hexapod for sample positioning and six strong in-vacuum permanent magnet quadrupoles to match the electron beam into the dielectric structure is installed in the switchyard to Athos and is currently being commissioned. It is also planned to demonstrate GV/m gradients in DLA structures with a length of 1 mm at a laser wavelength of 2 µm [13, 14].

Modulation and Bunching Diagnostics

We investigate methods to diagnose the energy modulation and temporal properties of the bunched electron beam after passing through the dielectric structure and magnetic chicane for compression. We outline a setup procedure to optimize spatial and temporal overlap between electrons and laser, as well as a method to precisely tune the modulation amplitude and compression factor to achieve the maximum peak current and shortest length of the individual spikes. Our calculations predict that an absolute measurement of the longitudinal phase-space with an rms-resolution of 350 as can be achieved with the planned X-band TDC at the end of the Athos beamline. The particle distribution used for this study is optimized with ASTRA [15] and ELEGANT [16] for the case of SwissFEL. The beam energy in the Athos beamline is 3 GeV. The normalized emittance (80 nm rad) at the core of the beam has been minimized for a charge of 30 pC.

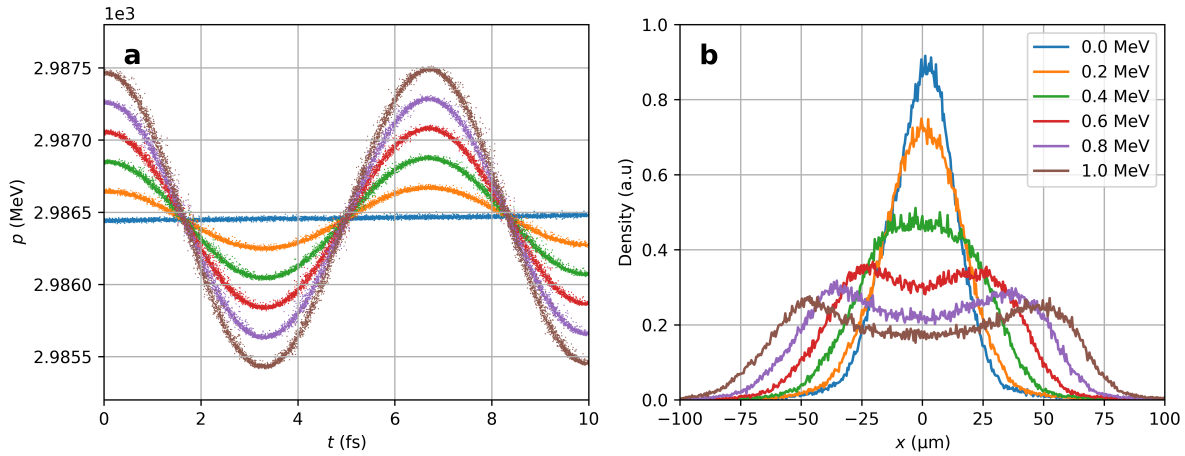

Figure 2. (a) 10-fs window of the modulated (uncompressed) longitudinal phase-space. (b) ELEGANT simulation of the horizontal electron distribution for different modulation strengths as seen on the dispersive screen in the Athos switchyard at SwissFEL. The characteristic double-horn structure which develops with increasing modulation strengths is observed.

Energy Spectrometer

A measurement of the increase in projected energy spread of the electron beam due to the laser interaction is needed to initially optimize spatial and temporal overlap between the laser pulse and the electrons in the dielectric structure. Since the total initial electron bunch length is longer than the wavelength of the laser (2 µm) the projected energy spread increases with the modulation amplitude. For the case of SwissFEL a suitable profile monitor is available in a dispersive section of the Athos switchyard. We perform tracking simulations with ELEGANT[16] for different modulation strengths and investigate the particle distribution at the location of the dispersive screen. The energy-modulated phase-space and the horizontal (x) projection are shown in Figure 2. The growth of the energy spread for increasing modulation strengths is clearly observable on the dispersive screen. A characteristic result of the projection of a sinusoidal modulation is the double-horn structure which develops for amplitudes exceeding the projected energy spread. The measurement of the energy spread can be used to infer the modulation amplitude, but no information about temporal properties of the electron beam is obtained.

Coherent Diffraction Radiation

A simple and non-invasive characterisation of the temporal bunch shape of the electron beam is the diagnosis of coherent diffraction radiation (CDR) emitted when the beam passes through a hole in a metallic foil. This concept is elaborated in [17, 18, 19, 20]. The spectral intensity of the CDR of N particles is related to the longitudinal bunch shape (longitudinal form factor), as described for instance in [21, 22, 23, 24], by

$$\frac{\mathrm{d}^2P}{\mathrm{d}\omega\mathrm{d}\Omega} = \frac{\mathrm{d}^2P_0}{\mathrm{d}\omega\mathrm{d}\Omega}(N + N(N-1)|F(\omega)|^2), \tag{1}$$

where $\mathrm{d}^2P_0/\mathrm{d}\omega\mathrm{d}\Omega$ is the single electron spectrum of the considered radiation process and F is the longitudinal form factor. This concept is also valid for other radiation processes which preserve the bunch shape, such as coherent transition or coherent synchrotron radiation. The

longitudinal form factor is given by the Fourier transform of the longitudinal charge distribution, neglecting the contribution of the transverse profile. The finite transverse extent of the beam will reduce the emitted intensity as investigated in [25]. This reduction can be minimized by focusing the electron beam into the radiator. In addition, we will concentrate the analysis on the CDR spectrum at wavelengths 15 to 40 times larger than the length of the individual spikes. For longer wavelength, compared to the bunch length, the effect of the transverse beam size is further suppressed. To estimate the radiation dependence on the modulation amplitude (for fixed compression, $R_{56} = 2\,\mathrm{mm}$), we calculate the current profile for a series of modulation amplitudes and simulate the emitted spectrum according to the derivation in [22].
Figure 3 contains the details of this scan. The longitudinal phase-space distribution is shown in sub-figure 3a for three characteristic cases (0.3 MeV: under-compressed, 0.5 MeV: fully compressed and 0.7 MeV: over-compressed). The corresponding current is given in the sub-figure below (3c). The simulated CDR spectrum emitted from a metallic foil with a hole (diameter: 1 mm) is plotted in sub-figure 3b. We neglect here radiation generated at other edges present in the beamline, for instance at diagnostic chambers. The mechanical design for a real machine should consider guiding and shielding of the electromagnetic radiation emitted at all edges and interfaces. The integrated spectrum (2 µm $\pm 1\,\%$) for the entire amplitude scan is shown in sub-figure 3d. In addition, we perform the same simulation scan for the case of a fixed modulation amplitude (0.5 MeV) and a variable compression factor R_{56}. The peak current and integrated CDR signal for both scans (amplitude and compression factor) are summarized in Figure 4. We observe that the intensity around the modulation wavelength (2 µm) is not monotonically correlated to the peak current of the bunch train. In the case of over-compression, the CDR signal keeps increasing, although the peak current is decreasing. This is a result of the increased 2 µm periodicity content in the Fourier transform of the current, while the peak current is already reduced.
To obtain more information about the length of the individual spikes, higher-order peaks of the CDR spectrum need to be taken into account as well. Figure 4 shows the CDR intensity at the central modulation wavelength (1st harmonic: 2 µm), at the 2nd and 3rd harmonic for both parameter scans. The spectrum at shorter wavelengths is indeed more sensitive to the length of the individual current spikes. This can be seen in the drop of the signal for over-compression for the higher harmonics. A key feature of the CDR simulation is the intersection of the normalized signals at the point of optimal compression. This reflects the fact that the current distribution is affected the most at the point where the linear part of the sinusoidal modulation is vertical in phase-space (close to optimal compression). Measuring the CDR spectrum during a scan of the modulation amplitude and the compression factor (R_{56}) and analysing their normalized intensities around fixed frequencies provides a simple optimization tool for the compression state of the bunch train.
Experimentally, this measurement can be realized by inserting a holed foil after the bunch compressor and transporting the radiation to a spectrometer or a series of wavelength-dependent beam splitters and photo-diodes, sensitive in the relevant spectral range (visible to near-infrared). A careful characterization of the detection setup is required and should include a measurement of the wavelength-dependent sensitivity as well as a test of the signal linearity with respect to the incident intensity. Therewith, single-shot acquisition permits to compare intensity ratios as depicted in Figure 4. To further increase the precision, beam-synchronous data acquisition would allow to take into account dependences on other beam parameters (e.g. charge and orbit fluctuations).

Transverse Deflecting Cavity
A direct measurement of the beam current can be achieved by correlating the longitudinal and transverse coordinates of the electron beam with the fields of a transverse deflecting cavity

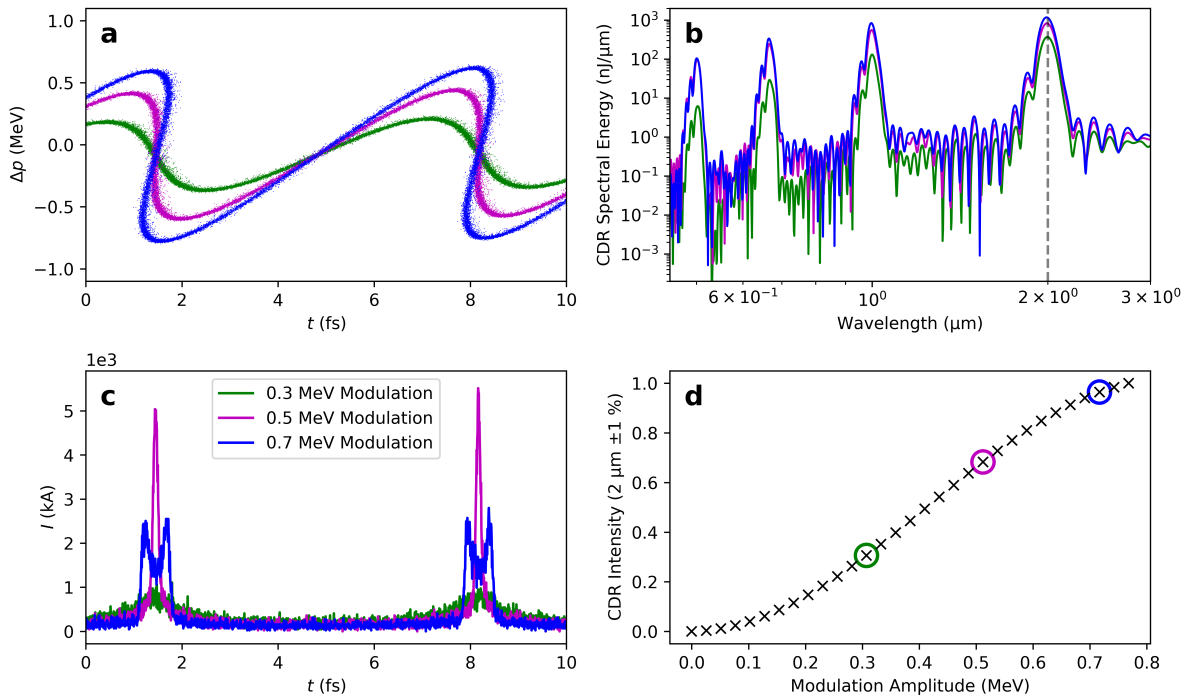

Figure 3. Phase-space (a) and beam current (c) of the modulated and compressed electron beam. The CDR emission spectrum comprises peaks at 2 µm (modulation wavelength) and at higher harmonics (b). The dependence of the integrated intensity on the modulation amplitude for a fixed compression factor within a range of ±1 % around 2 µm is shown in sub-figure (d).

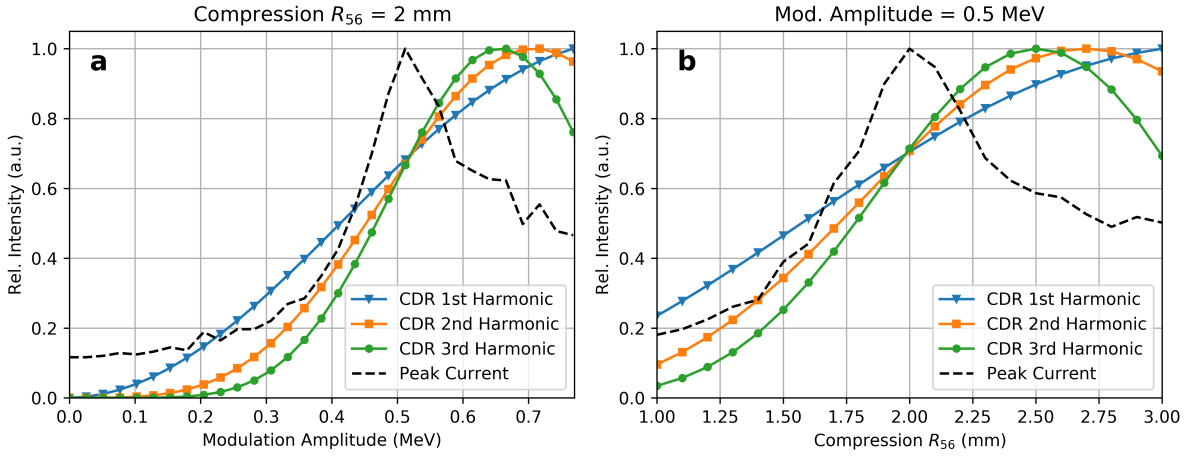

Figure 4. Normalized CDR signal at 2 µm and higher harmonics for two parameter scans: Left: modulation amplitude, Right: compression factor R_{56}. The CDR spectrum is integrated within a ±1 % interval. The peak current of the bunch train (after compression) is shown in black, dashed. The parameters for optimal compression coincide with the intersection of the CDR curves. At this point the slope of the CDR signals at all harmonics is maximal. Scanning the compression and modulation parameters while acquiring the intensity of the CDR spectrum provides a simple tool to maximize the current within the compressed bunch train.

(TDC). The longitudinal phase space can be retrieved by combining the TDC with a dispersive screen. A TDC with variable polarisation operating at X-band frequency is planned to be installed in the Athos beamline of SwissFEL [26]. Since the TDC will be in the post-undulator section, the measurement of the energy loss and energy-spread increase of the electron beam can be used to reconstruct the temporal profile of the photon pulses [27]. Sub-fs temporal resolution is expected by the post-undulator X-band TDC at Athos [26]. For a normalized emittance of 80 nm rad and a maximum RF voltage of 60 MV, our calculations predict an rms-resolution of 350 as. During the TDC streaking, the slice energy spread is expected to increase by about 0.4 MeV. This imposes a limit to the measurement of small energy modulations after the TDC.

Conclusion

We present simulations of diagnostic tools to characterize and optimize the modulation and compression for a bunch train obtained from dielectric laser modulation at SwissFEL. The energy modulation (without temporal information) can be observed and maximized in a dispersive screen in the Athos switchyard. The compressed bunch train can be characterized via CDR generated for instance at a hole in a metallic foil located after the magnetic chicane. Our simulations show that the peak current of the bunch train can be precisely optimized by measuring the CDR intensity at the modulation wavelength and a few higher harmonics while scanning the compression and modulation parameters. These diagnostic tools are investigated for electron bunch properties optimized for the DLA modulation scheme in the ACHIP chamber, but are applicable as well to similar electron pulse trains obtained by conventional undulator modulation for the ESASE scheme. These spectral diagnostics can be complemented by a TDC installed after the undulator, which can provide absolute temporal information of the electron and photons with an expected resolution of about 350 as.

References

[1] Ackermann W a, Asova G, Ayvazyan V, Azima A, Baboi N, Bähr J, Balandin V, Beutner B, Brandt A, Bolzmann A *et al.* 2007 *Nature photonics* **1** 336
[2] Allaria E, Badano L, Bassanese S, Capotondi F, Castronovo D, Cinquegrana P, Danailov M, D'Auria G, Demidovich A, De Monte R *et al.* 2015 *Journal of synchrotron radiation* **22** 485–491
[3] Emma P, Akre R, Arthur J, Bionta R, Bostedt C, Bozek J, Brachmann A, Bucksbaum P, Coffee R, Decker F J *et al.* 2010 *nature photonics* **4** 641
[4] Ishikawa T, Aoyagi H, Asaka T, Asano Y, Azumi N, Bizen T, Ego H, Fukami K, Fukui T, Furukawa Y *et al.* 2012 *nature photonics* **6** 540
[5] Altarelli M, Brinkmann R, Chergui M, Decking W, Dobson B, Düsterer S, Grübel G, Graeff W, Graafsma H, Hajdu J *et al.* 2006 *Technical design report, DESY* **97** 1–26
[6] Kang H S, Min C K, Heo H, Kim C, Yang H, Kim G, Nam I, Baek S Y, Choi H J, Mun G *et al.* 2017 *Nature Photonics* **11** 708
[7] Milne C, Schietinger T, Aiba M, Alarcon A, Alex J, Anghel A, Arsov V, Beard C, Beaud P, Bettoni S *et al.* 2017 *Applied Sciences* **7** 720
[8] Zholents A A 2005 *Physical Review Special Topics-Accelerators and Beams* **8** 040701
[9] England R J, Noble R J, Bane K, Dowell D H, Ng C K, Spencer J E, Tantawi S, Wu Z, Byer R L, Peralta E *et al.* 2014 *Reviews of Modern Physics* **86** 1337
[10] Hermann B, Bettoni S, Egenolf T, Niedermayer U, Prat E and Ischebeck R 2019 *Scientific Reports* **9** 1–9
[11] Abela R, Alarcon A, Alex J, Arrell C, Arsov V, Bettoni S, Bopp M, Bostedt C, Braun H H, Calvi M *et al.* 2019 *Journal of Synchrotron Radiation* **26**
[12] Thompson N and McNeil B 2008 *Physical review letters* **100** 203901
[13] Prat E, Bettoni S, Calvi M, Dehler M, Frei F, Hommelhoff P, Kozak M, McNeur J, Loch C O, Reiche S *et al.* 2017 *Nuclear Instruments and Methods in Physics Research Section A: Accelerators, Spectrometers, Detectors and Associated Equipment* **865** 87–90
[14] Ferrari E, Ischebeck R, Bednarzik M, Bettoni S, Borrelli S, Braun H H, Calvi M, David C, Dehler M, Frei F *et al.* 2018 *Nuclear Instruments and Methods in Physics Research Section A: Accelerators, Spectrometers, Detectors and Associated Equipment* **907** 244–247
[15] Floettmann K 2000 Astra `http://www.desy.de/~mpyflo/`

[16] Borland M 2000 Elegant: A flexible sdds-compliant code for accelerator simulation Tech. rep. Argonne National Lab., IL (US)
[17] Gerth C, Schmidt B, Wesch S, Ischebeck R, Orlandi G, Peier P and Schlott V 2011 *Proc. of DIPAC2011, Hamburg* 374–376
[18] Castellano M 1996 *Tesla Report 1996-08*
[19] Castellano M, Verzilov V, Catani L, Cianchi A, Orlandi G and Geitz M 2001 *Physical Review E* **63** 056501
[20] Chiadroni E 2006 *Tesla-FEL 2006-09*
[21] Frei F, Gorgisyan I, Smit B, Orlandi G, Beutner B, Prat E, Ischebeck R, Schlott V and Peier P 2013 *Proceedings of the 2nd International Beam Instrumentation Conference (IBIC 2013), Oxford, UK* pp 16–19
[22] Casalbuoni S, Schmidt B, Schmüser P and Steffen B 2005 *Tesla Report 2005-15*
[23] Lai R and Sievers A 1994 *Physical Review E* **50** R3342
[24] Lai R, Happek U and Sievers A 1994 *Physical Review E* **50** R4294
[25] Grimm O, Delsim-hashemi H, Bal V, Golubeva N *et al.* 2008 *Proceedings of EPAC08, Genoa, Italy, TUPC030*
[26] Craievich P, Reiche S, Ganter R, D'Arcy R, Prat E, Grudiev A, Wuensch W, Zennaro R, Christie F, McMonagle G *et al.* 2018 *38th International Free Electron Laser Conference FEL2017*
[27] Behrens C, Decker F J, Ding Y, Dolgashev V, Frisch J, Huang Z, Krejcik P, Loos H, Lutman A, Maxwell T *et al.* 2014 *Nature communications* **5** 3762